Differences in Dynamic Susceptibility Contrast MR Perfusion Maps Generated by Different Methods Implemented in Commercial Software

Laura Orsingher, PhD,† Silvia Piccinini, MD,‡ and Girolamo Crisi, MD‡*

Purpose: There are several potential sources of difference that can influence the reproducibility of magnetic resonance (MR) perfusion values. We aimed to investigate the reproducibility and variability of dynamic susceptibility contrast (DSC) MR imaging (MRI) parameters obtained from identical source data by using 2 commercially available software applications with different postprocessing algorithms.

Methods and Materials: We retrospectively evaluated DSC-MRI data sets of 24 consecutive patients with glioblastoma multiforme. Perfusion data were postprocessed with 2 commercial software packages, NordicICE (NordicNeuroLab, Bergen, Norway) and GE Brainstat (GE Healthcare, Milwaukee, Wis), each of which offers the possibility of different algorithms. We focused the comparison on their main analysis issues, that is, the gamma-variate fitting function (GVF) and the arterial input function (AIF). Two regions of interest were placed on maps of perfusion parameters (cerebral blood volume [CBV], cerebral blood flow [CBF], mean transit time [MTT]): one around tumor hot spot and one in the contralateral normal brain. A one-way repeated-measures analysis of variance was conducted to determine whether there was a significant difference in the calculated MTT, CBV, and CBF values.

Results: As regards NordicICE software application, the use of AIF is significant ($P = 0.048$) but not the use of GVF ($P = 0.803$) for CBV values. Additionally, in GE, the calculation method discloses a statistical effect on data. Comparing similar GE-NordicICE algorithms, both method ($P = 0.005$) and software ($P < 0.0001$) have a statistical effect in the difference. Leakage-corrected and uncorrected normalized CBV (nCBV) values are statistically equal. No statistical differences have been found in nMTT values when directly calculated. Values of nCBF are affected by the use of GVF.

Conclusion: The use of a different software application determines different results, even if the algorithms seem to be the same. The introduction of AIF in the data postprocessing determines a higher estimates variability that can make interhospital and intrahospital examinations not completely comparable. A simpler approach based on raw curve analysis produces more stable results.

Key Words: MR perfusion, software comparison, DSC-MRI, glioblastoma, CBV, CBF, MTT

(*J Comput Assist Tomogr* 2014;38: 647–654)

Dynamic susceptibility contrast (DSC) perfusion magnetic resonance imaging (MRI) (DSC-MRI) during bolus injection of gadolinium contrast agent is commonly used to investigate patients with primary brain tumors.[1–3] Cerebral blood volume (CBV) measurement derived from DSC-MRI has been shown to correlate with tumor grade and prognosis[4] and, recently, to provide a reliable estimation of the degree of neoangiogenesis, which could be useful for response assessment.[5,6] Longitudinal studies can benefit from quantitative analysis approaches; but in the case of DCS-MRI, the reliability of the absolute quantification can be affected by several potential source of errors: the accuracy of the arterial input function (AIF),[7,8] the delay and dispersion of bolus,[9,10] nonlinear dose response,[11,12] intersubject variability of hematocrit levels,[13] and choice of computational implementation of the model (such as the deconvolution method).[14] The long existing problem in MR quantitative imaging is that a criterion standard or a priori knowledge is needed for reference. Up to now, none of the proposed methods is free from pitfalls.[15] A cross correlation to a criterion standard technique (eg, positron emission tomography) has been proposed to calibrate the DSC-MRI measurement by calculating a scaling factor,[16] but, whereas this calibration provides consistent cerebral blood flow (CBF) values in normal subjects, its validity in pathological tissues is far from being definitely assessed.[13,17,18] Although a large number of studies have been performed on perfusion metrics, a single-standard postprocessing workflow has not been established and literature reported CBV values in brain tumors span a wide range,[1] from 4.72 ± 2.76 (n = 21) to 8.27 ± 2.0 (n = 6). Our study was aimed to investigate the variability and reproducibility with respect to the processing algorithms in the DSC-MRI estimates of perfusion parameters obtained from a group of patients with glioblastoma multiforme by using 2 commercially available software applications. Owing to all the aforementioned errors in quantification, we proposed to test if the reproducibility of results could be better with simpler postprocessing methods that rely only on the raw signal versus time curve. We also aimed to compare algorithms in similar principle but implemented in different software brands.

MATERIALS AND METHODS

Patients

We retrospectively evaluated DSC-MRI data sets of 24 consecutive patients with glioblastoma multiforme between October 2010 and March 2013. All these patients had undergone no surgery. Approval for this study protocol was obtained from the local institutional review board, and signed informed consent was acquired from all patients. A histopathologically confirmed diagnosis was obtained within 1 month after the MR study.

DSC-MRI

All MRI and DSC-MRI scans were performed on a 3-T whole-body scanner (Discovery MR 750; GE Healthcare, Milwaukee, Wis) equipped with an 8-channel phased-array head coil. Dynamic susceptibility contrast MRI data sets were acquired with gradient-echo-planar-imaging sequence after administration of a compact bolus of gadopentate dimeglumine by using an injection rate of 7 mL/s delivered via a power injector through an 18-gauge intravenous line. Dynamic susceptibility contrast MRI scan parameters were as follows: repetition time, 1500 milliseconds (ms); echo time, 30 ms; field of view, 24 cm; acquisition matrix, 128 × 128 (nominal

TABLE 1. Mathematical Details of the Postprocessing Methods

	CBV	MTT	CBF
ag	$\int_0^{t_1} C_t(t)\,dt$	$\dfrac{\int_0^{t_1} C_t(t)\,dt}{C_{peak}}$	CBF = CBV / MTT
aG$_{FM}$	$\int_0^{\infty} \Gamma(t)\,dt$	$\dfrac{\int_0^{\infty} \Gamma(t)\,dt}{C_{peak}}$	CBF = CBV / MTT
aG$_H$	$\int_0^{\infty} \Gamma(t)\,dt$	$\dfrac{\int_0^{\infty} t\cdot\Gamma(t)\,dt}{\int_0^{\infty} \Gamma(t)\,dt}$	CBF = CBV / MTT
AG$_N$	$\dfrac{\int_0^{\infty} \Gamma_t(t)\,dt}{\int_0^{\infty} \Gamma_a(t)\,dt}$	MTT = CBV / CBF	$CBF = \frac{k_h}{\rho}\max R(t)$
AG$_{RF}$	$\int_0^{\infty} R(t)\,dt$	MTT = CBV / CBF	$CBF = \frac{k_h}{\rho}\max R(t)$
Ag$_N$	$\dfrac{\int_0^{t_1} C_t(t)\,dt}{\int_0^{t_1} C_a(t)\,dt}$	MTT = CBV / CBF	$CBF = \frac{k_h}{\rho}\max R(t)$
Ag$_{RF}$	$\int_0^{\infty} R(t)\,dt$	MTT = CBV / CBF	$CBF = \frac{k_h}{\rho}\max R(t)$
BSGVF	$\int_0^{\infty} \Gamma(t)\,dt$	$\dfrac{\int_0^{\infty} t\cdot\Gamma(t)\,dt}{\int_0^{\infty} \Gamma(t)\,dt}$	CBF = CBV / MTT
BSAIF	$\dfrac{\int_0^{t_1} C_t(t)\,dt}{\int_0^{t_1} C_a(t)\,dt}$	$\int_0^{\infty} R(t)\,dt$	$CBF = \frac{k_h}{\rho}\max R(t)$

TABLE 1. *(Continued)*

	CBV	MTT	CBF
BSNEI	$\int_0^{t_1} C_t(t)\,dt$	Not calculated	Not calculated

Subscripts *t* and *a* refer to tissue and artery, respectively.

For abbreviation of methods, please refer to Figure 1.

$R(t)$, residue function; $\Gamma(t)$, gamma-variate fitting function; $C(t)$, signal intensity curve; C_{peak}, maximum height of the signal curve; ρ, tissue density; k_h, correction factor.

resolution, 1.8 mm); 22 contiguous 4-mm axial slices; and number of averages, 1. Sixty phases were acquired for 1320 images and a scan time of 90 seconds. The injection was delivered with a delay of 20 seconds.

Software Applications

Two commercially available software applications, NordicICE (Version 2.3.11, NordicNeuroLab, Bergen, Norway) and GE Brainstat (Functool 9.4.05, GE Healthcare, Milwaukee, Wis) are used at our institution for obtaining maps of DSC-MRI brain vascular estimates.

Preprocessing

The preprocessing steps aim to enhance the image quality and to correct for artifacts and specific properties of the blood. The GE software application has a predefined procedure, and we set the same options in NordicICE. All DSC-MRI images were corrected for motion. After a check on a subset of images with the χ^2 map of the curve-fitting procedure, we decided for no temporal smoothing and a spatial smoothing with a kernel size of 1.5 pixel. Initial images of the time series were excluded if transient signal intensity effects were present owing to a no-steady-state signal. The prebolus signal intensity was averaged and used as baseline. The raw signal can then be converted into relative change in R2* (ie, the change in the reciprocal of T2*) versus time.

Postprocessing

Both software applications can generate maps of the perfusion parameters (mean transit time [MTT], CBV, and CBF) on a voxel-by-voxel basis. Several approaches can be applied in the postprocessing procedure, but the main issue relies on whether the gamma-variate function (GVF) or AIF are used or not. For the mathematical details, refer to Table 1.

The GE software application offers the possibility to apply 3 different methods: BrainStatGVF (BSGVF), BrainStatAIF (BSAIF), and BrainStatNEI (BSNEI). As illustrated in Figure 1A, BSAIF implements the AIF deconvolution procedure, but the raw curves are not fitted to a GVF, and BSGVF fits the raw data with gamma-variate but does not consider the AIF.

In the NordicICE software application, all the postprocessing steps are independently implemented, and we composed the methods as schematized in Figure 1B. Each method has been labeled with the convention of using capital letter *A* if the AIF was used in the analysis and lower case *a* if not. The same is valid for the use or not of the GVF (*G* and *g*). When the first-pass dynamic curve is fitted to a GVF, images corresponding to the reperfusion peak were excluded.
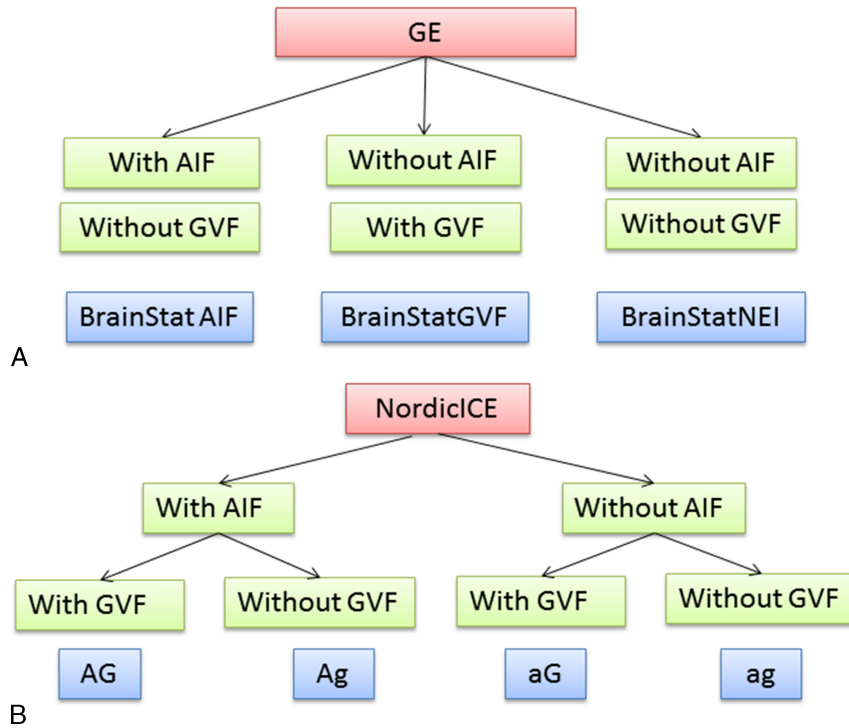
FIGURE 1. Graphic depiction of the postprocessing methods used with regard to their main characteristics. A, Description of the methods of the GE software application. B, Different methods we took into account for the NordicICE software application. Each method has been labeled with the convention of using capital letter *A* if the AIF is used in the processing and lower case *a* if not the case. The same is valid for the use or nonuse of the GVF (*G* and *g*). Figure 1 can be viewed online in color at www.jcat.org.

When no AIF deconvolution is applied, we can only perform a raw dynamic curve analysis. Cerebral blood volume is estimated from the area under the first-pass curve (AUC), whereas MTT can be calculated with the "area-to-height" relation (aG_H method)[19,20] or the "first moment" approach (aG_{FM} method).[20] Cerebral blood flow can be calculated only as a ratio of the other 2 parameters.

When the AIF function is detected, CBF is calculated directly from the convolution of the AIF input function and the residue function. Cerebral blood volume can be calculated with 2 algorithms (CBValg): it can be computed by area normalization, that is, the ratio of the area under the signal versus time curve divided by the area under the AIF (AG_N method), or it can also be estimated from the area under the residue function curve (AG_{RF} method).

In both software applications, the positions of AIF were set in a semiautomatic way: AIF pixels are automatically selected in a user-defined region of interest (ROI) at the insular segment of the middle cerebral artery on the unaffected side. Positioning was performed carefully to ensure consistency among the methods.

For what concerns the deconvolution procedure, we used the truncated singular value deconvolution[14,21] with fixed threshold level of 0.2 as cutoff value for diagonal elements in the NordicICE to correspond to the implemented procedure in GE.

In NordicICE, contrast agent leakage correction can be applied to data using the method proposed by Boxerman.[22,23] Two pairs of CBV maps have been calculated with the use of AIF deconvolution and GVF, one with the normalization approach (AG_{Nbis} method) and the other pair with the residue function implementation (method AG_{RFbis}). For both of them, corrected and uncorrected values on a pixel-by-pixel basis have been produced. In the GE software application, this option is not implemented.

Data Collection

Regions of interest were manually constructed by a neuroradiologist (with more than 3 years of experience) using the contrast-enhanced T1-weighted image as reference. Two ROIs of the same area were placed: one around tumor hot spot and the other one in the contralateral normal white matter. The same ROIs for a given patient were used across all the postprocessing methods. Each ROI-averaged CBV, CBF, and MTT estimate was then normalized (nCBV, nCBF, and nMTT) to the corresponding ROI-averaged values in the normal brain white matter. Values from the ROIs placed in normal brain white matter were also recorded. In the following, we will use the abbreviation nCBV to indicate the ratio CBV (tumor) / CBV (controlateral normal-appearing white matter) and rCBV to indicate values as they come from the postprocessing procedure.

Statistical Analysis

All statistical analyses were performed with IBM SPSS (Version 18.0; Statistical Package for the Social Sciences, Chicago, IL). After having verified the normality, homoscedasticity and sphericity of the data, a one-way repeated-measures analysis of variance (ANOVA) was conducted to determine whether there was a significant difference in the calculated perfusion estimates. Factorial analysis has been applied to investigate which independent variables have significant effects. Moreover, post hoc Bonferroni test, with the correction of significance in case of multiple comparisons, was applied to determine which couple of methods has produced this significant difference. Significance was set at $P < 0.05$. We compare the statistical differences among

methods with regard to the 3 physiological parameters bearing in mind that they are not independent but linked by the central volume principle. Statistical comparison have been performed only on estimates coming from direct calculation, in particular, CBF when AIF is used in the data processing procedure and MTT in the raw curve analysis. Coefficients of variation (CVs) of the mean values were also calculated.

RESULTS

All the perfusion parameter (MTT, CBV, and CBF) maps were successfully generated on a voxel-by-voxel basis by using
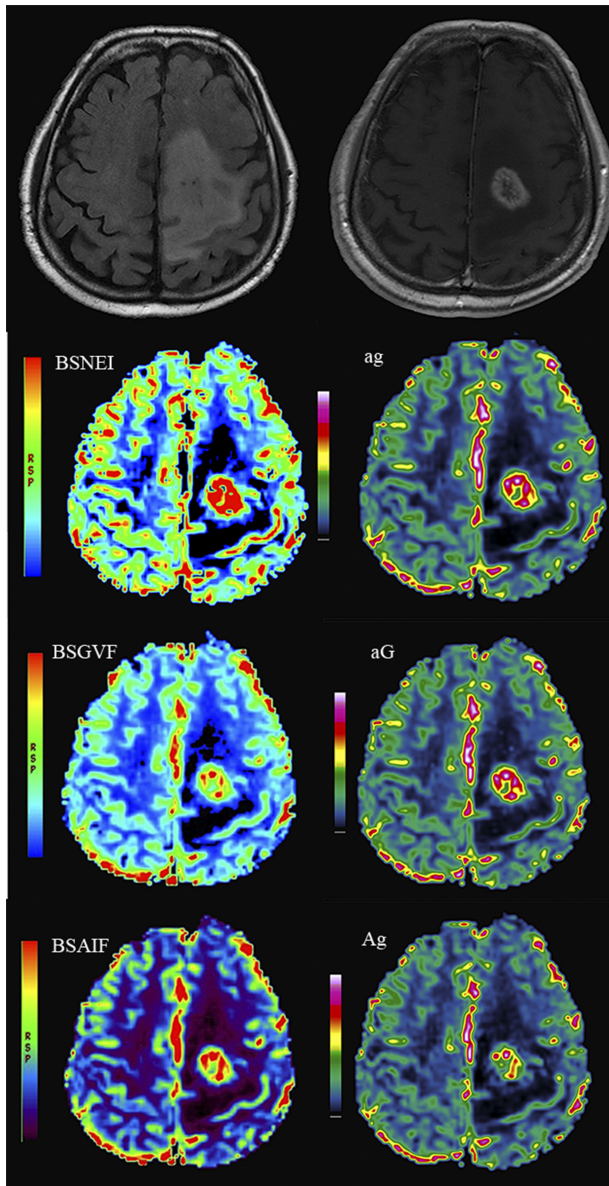

FIGURE 2. First row: axial T2–fluid-attenuated inversion recovery and T1-weighted contrast-enhanced images of left posterior frontal glioblastoma multiforme. Lower rows: parametric maps for nCBV generated with GE software application (left) and NordicICE software (right). Similar methods were grouped in rows. NordicICE method, which is the most similar to BSGVF, is the aG, whereas BSAIF can be well matched with Ag_{RF} method. The ag method can be compared to BSNEI. Figure 2 can be viewed online in color at www.jcat.org.

10 postprocessing methods. Typical CBV maps generated with 6 different methods are shown in Figure 2.

Figure 3 displays nCBV, nCBF, and nMTT values as a function of postprocessing method. The box plots show the median values for each group (middle line), with the box representing the 75th and 25th percentile values from top to bottom, respectively. The same data are also summarized in Table 2, where the mean, standard deviation (SD), and range of data are listed for all methods.

Normalized CBV values are always positive for all postprocessing methods. The mean values of nCBV range from a minimum of 5.77 to a maximum of 8.79. The lowest mean we found is given by the BSNEI method. The minimum value ever obtained is 1.54, and the maximum one is 27.96; both come from the Ag_{RF} method. Ag_{RF} method displays also the maximum SD in nCBF values. Normalized MTT and nCBF data show similar CVs of mean values (34%), whereas nCBV has a CV of 20%.

Taking into account all 10 methods, the Mauchly test indicates that the assumption of sphericity has been violated ($\eta^2 = 352$, $P < 0.001$). Therefore, degrees of freedom are corrected using the Greenhouse-Geisser estimate of sphericity ($\varepsilon = 0.33$). One-way repeated-measures ANOVA indicates that there is at least one couple of postprocessing methods statistically different: $F(9, 21) = 7.44$; $P < 0.001$; $\eta^2 = 0.24$. It should be noted, however, that the number of comparisons for each possible matched pairs is high with respect to the numerosity of the sample. Therefore, to understand better where the cause of the variability of the data is, we combined methods that share some similarities.

The NordicICE software offers the possibilities to take into account separately the effect of the use of AIF and GVF in the CBV calculation. Factorial ANOVA test indicates that there is a significant effect of the use of AIF in the calculated nCBV values: $F(1,23) = 4.32$; $P = 0.04$; $\eta^2 = 0.16$. The use of GVF has no significant effects, $F(1, 23) = 0.06$; $P = 0.80$; $\eta^2 = 0.03$. There is no interaction between the 2 factors: $F(1, 23) = 0.20$; $P = 0.66$; $\eta^2 = 0.08$. Among the methods, which rely on the AIF detection (AG_N, AG_{RF}, Ag_N, and Ag_{RF}), the use of GVF is still not significant: $F(1, 23) = 0.12$; $P = 0.73$; $\eta^2 = 0.005$, as it is the CBValg (based on the residue function or on the normalized intensity curve), $F(1, 23) = 3.25$; $P = 0.08$; $\eta^2 = 0.124$. There is no interaction between the 2 factors: $F(1, 23) = 0.03$; $P = 0.86$; $\eta^2 = 0.001$. Normalized CBV values, obtained from methods with AIF, range from 7.39 ± 2.90 to 8.79 ± 5.01, with a CV of 15%. The CV for methods without AIF is 2%. With regard to the GE software application, the calculation method has a significant effect: $F(2, 46) = 9.54$; $P < 0.001$; $\eta^2 = 0.29$. Pairwise comparisons indicate that there is a significant difference between BSAIF and BSNEI ($P = 0.005$; mean difference, 2.88; 95% confidence interval [CI], 0.81–4.95) and also between BSGVF and BSNEI ($P = 0.005$; mean difference, 1.93; 95% CI, 0.53–3.32).

The NordicICE aG method is the most similar to BSGVF, whereas BSAIF can be well matched with Ag_{RF} method. The ag method can be compared to BSNEI. The ANOVA test performed on the aforementioned 6 methods indicates that both the method ($F(2, 46) = 6.07$, $P = 0.005$; $\eta^2 = 0.209$) and software brand ($F(1, 23) = 19.3$; $P < 0.0001$; $\eta^2 = 0.46$) are statistically significant in nCBV values. There is no interaction between the 2 factors ($P = 0.165$). In particular, a pairwise comparison on the couples of similar methods shows that the methods with AIF show statistical difference, whereas the methods with the GVF yield similar results in nCBV indices.

With regard to nCBF estimates, we took into account AG_N, Ag_{RF}, Ag_N, and AG_{RF} from NordicICE and BSAIF from GE. After ANOVA test, $F(4, 92) = 15.13$; $P < 0.001$; $\eta^2 = 0.40$, the Bonferroni test indicates that the couples of methods listed
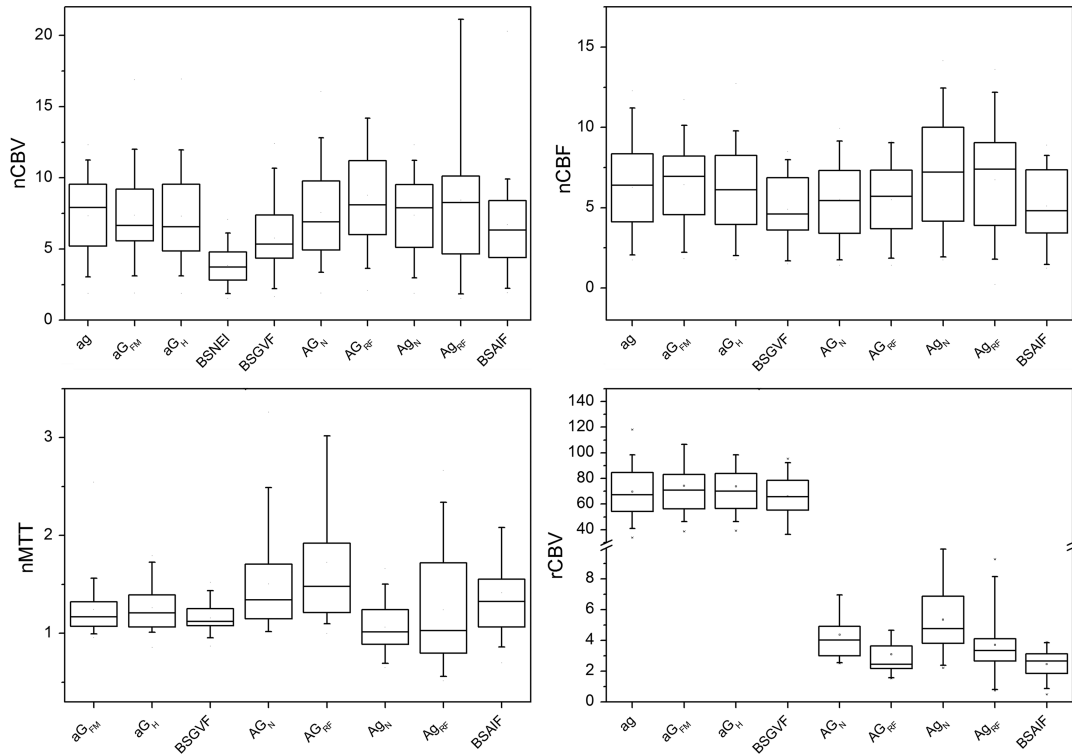
FIGURE 3. Normalized CBV, nCBF, and nMTT values as a function of postprocessing methods. The box plots show the median values for each method (middle line) with the box representing the 75th and 25th percentile values from top to bottom, respectively. Box plots for rCBV of white matter values in institutional units are also shown.

in Table 3 have statistical differences. The CV in nCBF values for methods with AIF is 50%, whereas without AIF, the CV is 30%.

The ag, aG_{FM}, aG_H, and BSGVF methods do not rely on the detection of AIF, and MTT is directly calculated. The one-way ANOVA test does not disclose any statistical difference in the MTT values.

Leakage Correction

The percentage difference (magnitude of difference divided by mean) between corrected and uncorrected nCBV was computed.

The percentage differences are (minimum, maximum, and mean): 0, 2.55, and 0.89 for $nCBV_N$ and 0, 7.86, and 1.41 for $nCBV_{RF}$. Paired *t* tests on couples AG_{RF}/AG_{RFbis} and AG_N/AG_{Nbis} do not show any statistical difference.

Normal Values in "Institutional Units"

We also performed statistical analysis on the "absolute" outcomes of the methods. Bearing in mind that quantification in absolute units is difficult to achieve, we can always think in terms of "institutional units". Box plots for "institutional" values of rCBV for normal-appearing white matter are shown in Figure 3.

TABLE 2. Results for nCBV, nCBF, and nMTT for Glioblastomas

	nCBV				nCBF				nMTT			
	Mean	**SD**	**Min**	**Max**	**Mean**	**SD**	**Min**	**Max**	**Mean**	**SD**	**Min**	**Max**
ag	7.35	2.95	1.89	12.33	6.27	2.91	1.76	12.29	1.26	0.40	0.62	2.89
aG_{FM}	7.38	3.31	1.90	16.90	6.44	2.71	1.83	11.74	1.25	0.32	0.96	2.54
aG_H	7.31	3.37	1.90	16.96	6.14	2.84	1.78	12.73	1.26	0.24	0.86	1.79
BSNEI	3.84	1.40	1.54	7.09	—	—	—	—	—	—	—	—
BSGVF	5.77	2.59	1.67	12.42	4.92	1.93	1.51	8.50	1.16	0.15	0.87	1.52
AG_N	7.56	3.31	1.90	16.08	5.52	2.53	1.43	9.95	1.50	0.53	1.02	3.26
AG_{RF}	8.79	5.01	2.10	27.37	5.50	2.38	1.43	9.16	1.73	0.80	1.00	4.44
Ag_N	7.39	2.90	1.90	12.34	7.25	3.59	1.76	13.61	1.07	0.26	0.65	1.66
Ag_{RF}	8.45	5.97	1.54	27.96	6.74	3.52	0.22	14.16	1.24	0.60	0.52	2.67
BSAIF	6.72	3.67	1.94	20.31	5.11	2.28	1.25	8.91	1.42	0.61	0.70	3.83

The prefix *n* indicates that the values are ratios of rCBV (tumor) / rCBV (contralateral normal white matter). For abbreviation of methods, please refer to Figure 1.

Max, maximum value in the group; min, minimum value in the group; SD, standard deviation of data.

TABLE 3. List of Couples of Methods That Show Statistical Differences With Respect to nCBV, nCBF, and nMTT

nCBV	nCBF	nMTT
	AG_N and Ag_N	AG_N and Ag_N
	Ag_{RF} and AG_{RF}	Ag_{RF} and AG_{RF}
	Ag_N and AG_{RF}	Ag_N and AG_{RF}
	Ag_{RF} and BSAIF	
	Ag_N and BSAIF	Ag_N and BSAIF
AG_{RF} and BSAIF		AG_{RF} and BSAIF
		AG_N and AG_{RF}

The factorial ANOVA test indicates that there is a significant effect of the use of AIF in the calculated rCBV values, $F(1,23) = 89.846$; $P < 0.0001$; $\eta^2 = 0.796$. The use of gamma has no significant effects, $F(1,23) = 1.018$; $P = 00.323$; $\eta^2 = 0.042$. There is no interaction between the 2 factors, $F(1,23) = 1.951$; $P = 0.176$; $\eta^2 = 0.078$. If we divide the methods into 2 groups with respect to the application or no application of the AIF in the postprocessing, pairwise comparisons for the effects of AIF with a Bonferroni adjustment indicates that there is a significant difference between the methods with and without AIF ($P < 0.0001$; mean difference, 485; 95% confidence interval for difference, 379–590). Moreover, if we focus our attention only on the methods with gamma and without AIF, we see that the methods do not present statistical differences in the distribution of the rCBV values. On the other hand, if we check the existence for statistical differences among the methods with AIF, we have at least one couple of methods that is statistically different: $F(3, 69) = 14.15$; $P < 0.0001$; $\eta^2 = 0.381$.

DISCUSSION

Considerable evidence has been accumulated during the last few years that DSC-MRI can provide valuable clinical data concerning tumor grading,[24,25] tumor progression,[26,27] and therapy response monitoring.[28,29] In this respect, intervendor software effects on data reproducibility have to be taken into account.[30,31] To eliminate interoperator variability, which can act as a covariate in the algorithms comparison,[31] ROIs have been always placed by the same neuroradiologist with the supervision of another well-experienced neuroradiologist. However, our nCBV estimates, ranging from 3.84 ± 1.40 to 8.79 ± 5.01 in 24 patients, display a wide range of mean values and reflect the variability found in the literature.

As previously reported,[30,31] software differences constitute the primary source of variability in perfusion parameters, and specific strategies should be optimized with respect to different clinical needs. In both software applications, AIF has an important influence on data. In NordicICE, AIF has a statistical effect among GE methods; although we could not investigate mutual influence of GVF and AIF, the effect of AIF seems to be greater than GVF. Moreover, our results show that the introduction of AIF in the data postprocessing introduces higher values variability.

The DSC-MRI measurements assume that the contrast agent remains intravascular, but in case of disruption or absence of the blood-brain barrier such as in brain malignant tumors, an extravasation to extravascular tissue space takes place. NordicICE offers the possibility to produce CBV leakage-corrected maps. Unlike the case reported in Toh et al,[32] we did not find any statistical difference between the corrected and uncorrected nCBV maps in our group of GBMs. The results from Toh et al show that the mean

CBV ratio and corrected CBV ratio are 1.16 ± 0.66 and 2.28 ± 0.60, respectively for primary central nervous system lymphoma and were 5.00 ± 2.00 and 5.47 ± 2.05, respectively for GBM. This means that whereas for primary central nervous system lymphomas, the corrected maps have almost double values in the case of GBM, the difference is definitely lower. Moreover, we found a mean percent difference between corrected and uncorrected maps of the same order of magnitude as in Toh et al[32] (less than 10%). The "Boxerman correction," performing linear fitting of the experimental data, moderates the effects of contrast agent extravasation on T2*-weighted signal intensity loss. The extravasated contrast agent has 2 competing effects on the extravascular compartment: a corrupting T2 contrast drop and a T1 enhancement. The proposed rCBV correction is robust in the presence of this effect. Moreover, the fitting-correction technique takes the entire raw dynamic curve into account, increasing the fitting performance. Additionally, the gamma-variate fitting techniques can correct the tail deviation of $\Delta R2(t)$ caused by contrast leakage, forcing the postbolus $\Delta R_2(t)$ back to baseline. This fitting of experimental signal curve can reduce the overestimation owing to contrast agent recirculation and can help eliminate the effects of leakage into the extravascular space. Our results demonstrate a sufficient leakage correction by GVF. Moreover, different conclusions have been drawn in the past on the use of corrected and uncorrected maps. For example, in Toh et al[32] authors show that the uncorrected rCBV values have the best diagnostic performance compared to the corrected ones.

It should be noted that if longitudinal studies have to be performed, an accurate but unstable result could not be the best solution. In this context, the effects of software automation have to be taken into account. Our findings show that when the same algorithm and the same software in the CBV calculation are applied, equivalent results are obtained. This can be regarded as a proof of the reproducibility of data processing workflow in NordicICE with regard to AIF automatic detection, GVF, and deconvolution. On the other hand, nCBV estimates are affected by the use of a different software application, even if the algorithms seem to be the same, so that MR perfusion results cannot be directly generalized from one vendor software to another.

If conflicting findings can be obtained using different software on same source data, all the more so if we compare results obtained at different institutions. Bjørnerud and Emblem[33] have also investigated statistical differences on the nCBV calculation. They compared 2 different approaches: model 1, similar to our AG_N method; and model 2, similar to our AG_{RF} method. They found that model 1 gives significantly higher nCBV values compared with model 2 for all deconvolution methods. On the contrary, our results show that CBValg has no statistical effects in the data variance. This difference can arise from the AG_{RF} method calculation of nCBV as integration from the residue function and not as the product of CBF and MTT. In our analysis, same data are produced if we calculate directly nCBV as peak integration of the tissue over AIF curve or with the residue function integration. This demonstrates the experimental equality of the following relation:

$$F \int R(t)dt = \frac{\int C_t(t)dt}{\int C_a(t)dt}$$

Method 1 may lead to overestimation of nCBV owing to recirculation effects in the tissue signal curve, but our results demonstrate that when GVF is used, the recirculation effects are sensibly reduced. This is consistent also with our results on

leakage maps, where there are no statistical differences between leakage-corrected and uncorrected nCBV.

A single postprocessing step can have different effects on each perfusion parameter. Our results show that the fitting procedure of the raw data curve with the GVF has no effects on nCBV values, whereas the methods that show statistical differences with respect to nCBF values are only differentiated by the use or non-use of GVF. In fact, the fitting procedure of raw curves with gamma-variate function, assuming that the dynamic tissue curve has a predefined shape,[34] reduces effects of spikes in the first-pass curve, and AUC is given analytically without the need for numerical integration to determine nCBV. The GVF method is less dependent than AIF to quantification issues and does not introduce hypothesis on T1, T2 relativity of blood, healthy, and tumor tissues. The processing is more straightforward from raw curve signal to nCBV estimation so that nCBV maps computed with different software do not show significant differences.

On the other hand, CBF is calculated as the maximum of the RF curve. An integral procedure, intrinsically averaging noise oscillations, is less sensitive to spikes than a peak value determination. The DSC-MRI technique can provide, in principle, the perfusion indices CBF, CBV, and MTT in absolute unit once the arterial and tissue signals are experimentally determined in identical units. This, however, poses a number of practical problems. First, the relaxation rate is proved to deviate from a linear proportionality to the intravascular concentration of contrast agent. Moreover, we have to use constant values for hematocrit in large and small vessels and to assume a uniform relativity effect of the contrast agent for all tissues, normal or pathological ones. Another concern arises from the distance between the place where the AIF is measured and the downstream tissue element, where the shape of the input function becomes dispersed and delayed.

In addition to the difference of the GVF effect on nCBV and nCBF, the applied methods disclose different behavior also in data SD. Considering the methods with AIF, SDs in nCBF values are higher than SDs in nCBVs. The reason could be ascribed to the different calculation possibilities: nCBF is directly calculated via deconvolution process, whereas nCBV can be calculated in 2 different ways (normalization procedure or residue function approach).

The statistical differences found in nCBF values impinge on the nMTT values calculated at CBV/CBF ratio; on the other hand, when MTT is directly calculated, all methods provide homogenous nMTT values. This can be easily explained by the MTT measurement, which comes directly in seconds without any data manipulation, and it does not rely on the intensity of the curve. Moreover, it should be noted that for absolute quantification of CBV and CBF, scaling factors are fundamental. Cerebral blood volume and CBF can therefore be provided in relative units (institutional units) while, since the same scaling factors affect both CBV and CBF, they cancel out in MTT. This observation should encourage the direct determination of MTT in all cases to check the consistency between the other 2 perfusion parameters and to correct them accordingly.

The combined effects of all the important steps in the CBV calculation are summarized in the Ag_{RF} method. It displays the highest value variability in nCBV (SD, 70%), which can be related to the use of AIF and the absence of the gamma-variate fitting procedure.

Bearing in mind that an absolute quantification is beyond the scope of this work, we can test the variability of institutional data of normal white matter with respect to the postprocessing method. This can help to minimize the variability of data associated with pathology and to eliminate possible effects of leakage on tissue signal curve intensity. Interestingly, among the methods with the use of a gamma-variate fitting, there is no significant difference.

Conversely, the methods with the detection of AIF show statistical differences. This reflects the same situation as the normalized tumor values.

This study had some limitations. First, acceptable limits of variability in perfusion results were not considered. A healthy control group was not included. Abnormal hemodynamic properties of tumor tissue can affect the data variability independently from postprocessing algorithms. Another limitation arises from the fact that we compare commercially available software without the possibility to investigate in detail all the calculation steps such as, for example, the impact of different noise threshold for singular-value-decomposition or specific algorithm for AIF automatic detection. Moreover, no effects on perfusion parameters due to acquisition sequence or examination procedure have been considered.

In summary, our work aimed to compare fast and fully automated quantitative perfusion analysis methods implemented in 2 different software brands. Different vendor software applications lead to nonequivalent perfusion values, even if the algorithms seem to be the same. The introduction of AIF in the data postprocessing determines higher estimates of variability. On the other hand, the gamma fitting procedure can sufficiently correct for leakage and yields more reproducible results when different algorithms and different vendors are compared.

In the case of interhospital and intrahospital examination comparison, the preferable solution is to use a simpler approach based on raw curve analysis because quantification processes lead to results not completely comparable even if the ratio of tumor to normal values is considered.

REFERENCES

1. Knopp EA, Cha S, Johnson G, et al. Glial neoplasms: dynamic contrast-enhanced T2*-weighted MR imaging. *Radiology*. 1999;211: 791–798.

2. Lam WW, Chan KW, Wong WL, et al. Pre-operative grading of intracranial glioma. *Acta Radiol*. 2001;42:548–554.

3. Kremer S, Grand S, Remy C, et al. Cerebral blood volume mapping by MR imaging in the initial evaluation of brain tumors. *J Neuroradiol*. 2002;29:105–113.

4. Aronen H, Gazit I, Louis D, et al. Cerebral blood volume maps of gliomas: comparison with tumor grade and histologic findings. *Radiology*. 1994; 191:41–51.

5. Sugahara T, Korogi Y, Kochi M, et al. Correlation of MR imaging determined cerebral blood volume maps with histologic and angiographic determination of vascularity of gliomas. *AJR Am J Roentgenol*. 1998;171:1479–1486.

6. Aronen H, Pardo F, Kennedy DN, et al. High microvascular blood volume is associated with high glucose uptake and tumor angiogenesis in human gliomas. *Clin Cancer Res*. 2000;6:2189–2200.

7. van Osch MJP, Vonken EPA, Viergever MA, et al. Measuring the arterial input function with gradient echo sequences. *Magn Reson Med*. 2003;49:1067–1076.

8. Carroll TJ, Rowley HA, Haughton VM. Automatic calculation of the arterial input function for cerebral perfusion imaging with MR imaging. *Radiology*. 2003;227:593–600.

9. Calamante F, Gadian D, Connelly A. Delay and dispersion effects in dynamic susceptibility contrast MRI; simulations using singular value decomposition. *Magn Res Med*. 2000;44:1–8.

10. Calamante F. Bolus dispersion issues related to the quantification of perfusion MRI data. *J Magn Reson Imaging*. 2005;22:718–722.

11. Johnson KM, Tao JZT, Kennan RP, et al. Intravascular susceptibility agent effects on tissue transverse relaxation rates in vivo. *Magn Reson Med*. 2000;44:909–914.

12. Kiselev VG. On the theoretical basis of perfusion measurements by dynamic susceptibility contrast MRI. *Magn Reson Med*. 2001;46:1113–1122.

13. Calamante F, Gadian DG, Connelly A. Quantification of perfusion using bolus tracking MRI in stroke. Assumptions, limitations, and potential implications for clinical use. *Stroke*. 2002;33:1146–1151.

14. Wirestam R, Andersson L, Østergaard L, et al. Assessment of regional cerebral blood flow by dynamic susceptibility contrast MRI using different deconvolution techniques. *Magn Reson Med*. 2000;43:691–700.

15. Knutsson L, Ståhlberg F, Wirestam R. Absolute quantification of perfusion using dynamic susceptibility contrast MRI: pitfalls and possibilities. *Magn Reson Mater Phy*. 2010;23:1–21.

16. Ostergaard L, Smith DF, Vestergaard-Poulsen P, et al. Absolute cerebral blood flow and blood volume measured by magnetic resonance imaging bolus tracking: comparison with positron emission tomography values. *J Cereb Blood Flow Metab*. 1998;18:425–432.

17. Sorensen AG. What Is the Meaning of Quantitative CBF? *AJNR Am J Neuroradiol*. 2001;22:235–236.

18. Lin W, Celik A, Derdeyn C, et al. Quantitative measurements of cerebral blood flow in patients with unilateral carotid artery occlusion: a PET and MR study. *J Magn Reson Imaging*. 2001;14:659–667.

19. Axel L. Cerebral blood flow determination by rapid-sequence computed tomography. *Radiology*. 1980;137:679–686.

20. Fieselmann A, Kowarschik M, Ganguly A, et al. Deconvolution-based CT and MR brain perfusion measurement: theoretical model revisited and practical implementation details. *Int J Biomed Imaging*. 2011;14:1–20.

21. Kudo K, Sasaki M, Østergaard L, et al. Susceptibility of Tmax to tracer delay on perfusion analysis: quantitative evaluation of various deconvolution algorithms using digital phantoms. *J Cereb Blood Flow Metab*. 2011;31:908–912.

22. Weisskoff RM, Zuo CS, Boxerman JL, et al. Microscopic susceptibility variation and transverse relaxation. Theory and experiment. *Magn Reson Med*. 1994;31:601–610.

23. Boxerman JL, Schmainda KM, Weisskoff RM. Relative cerebral blood volume maps corrected for contrast agent extravasation significantly correlate with glioma tumor grade, whereas uncorrected maps do not. *AJNR Am J Neuroradiol*. 2006;27:859–867.

24. Covarrubias DJ, Rosen BR, Lev MH. Dynamic magnetic resonance perfusion imaging of brain tumors. *Oncologist*. 2004;9:528–537.

25. Law M, Oh S, Johnson G, et al. Perfusion magnetic resonance imaging predicts patient outcome as an adjunct to histopathology: a second reference standard in the surgical and nonsurgical treatment of low-grade gliomas. *Neurosurgery*. 2006;58:1099–1107.

26. Law M, Young RJ, Babb JS, et al. Gliomas: predicting time to progression or survival with cerebral blood volume measurements at dynamic susceptibility-weighted contrast-enhanced perfusion MR imaging. *Radiology*. 2008;247:490–498.

27. Bisdas S, Kirkpatrick M, Giglio P, et al. Cerebral blood volume measurements by perfusion-weighted MR imaging in gliomas: ready for prime time in predicting short-term outcome and recurrent disease? *AJNR Am J Neuroradiol*. 2009;30:681–688.

28. Gerstner ER, Sorensen AG, Jain RK, et al. Advances in neuroimaging techniques for the evaluation of tumor growth, vascular permeability, and angiogenesis in gliomas. *Curr Opin Neurol*. 2008;21:728–735.

29. Hirai T, Murakami R, Nakamura H, et al. Prognostic value of perfusion MR imaging of high-grade astrocytomas: long-term follow-up study. *AJNR Am J Neuroradiol*. 2008;29:1505–1510.

30. Kudo K, Sasaki M, Yamada K, et al. Differences in CT perfusion maps generated by different commercial software: quantitative analysis by using identical source data of acute stroke patients. *Radiology*. 2010;254:200–209.

31. Zussman BM, Boghosian G, Gorniak RJ, et al. The relative effect of vendor variability in ct perfusion results: a method comparison study. *AJR Am J Roentgenol*. 2011;197:468–473.

32. Toh CH, Wei KC, Chang CN, et al. Differentiation of primary central nervous system lymphomas and glioblastomas: comparisons of diagnostic performance of dynamic susceptibility contrast-enhanced perfusion MR imaging without and with contrast-leakage correction. *AJNR Am J Neuroradiol*. 2013;34:1145–1149.

33. Bjørnerud A, Emblem KE. A fully automated method for quantitative cerebral hemodynamic analysis using DSC–MRI. *J Cereb Blood Flow Metab*. 2010;30:1066–1078.

34. Davenport R. The derivation of the gamma-variate relationship for tracer dilution curves. *J Nucl Med*. 1983;24:945–948.